Applied Physics Letters

Single-particle states spectroscopy in individual carbon nanotubes with an aid of tunneling contacts

Cite as: Appl. Phys. Lett. **120**, 083104 (2022); https://doi.org/10.1063/5.0080093
Submitted: 29 November 2021 • Accepted: 07 February 2022 • Published Online: 24 February 2022

Yakov Matyushkin, Maxim Moskotin, Yuriy Rogov, et al.

Applied Physics Letters ARTICLE scitation.org/journal/apl

Single-particle states spectroscopy in individual carbon nanotubes with an aid of tunneling contacts

Cite as: Appl. Phys. Lett. **120**, 083104 (2022); doi: 10.1063/5.0080093
Submitted: 29 November 2021 · Accepted: 7 February 2022 ·
Published Online: 24 February 2022

Yakov Matyushkin,[1,2,3] Maxim Moskotin,[1,2] Yuriy Rogov,[1] Aleksandr Kuntsevich,[4] Gregory Goltsman,[2,3] and Georgy Fedorov[1,a)]

AFFILIATIONS

[1]Moscow Institute of Physics and Technology, Dolgoprudny 141700, Russia
[2]Moscow Pedagogical State University (MPSU), Moscow 119435, Russia
[3]National Research University Higher School of Economics, Moscow 101000, Russia
[4]P. N. Lebedev Physical Institute, Russian Academy of Sciences, Moscow 119991, Russia

[a)]Author to whom correspondence should be addressed: fedorov.ge@mipt.ru

ABSTRACT

Recent studies have demonstrated that the band structure of a carbon nanotube (CNT) depends not only on its geometry but also on various factors such as atmosphere chemical composition and dielectric environment. Systematic studies of these effects require an efficient tool for an *in situ* investigation of a CNT band structure. In this work, we fabricate tunneling contacts to individual semiconducting carbon nanotubes through a thin layer of alumina and perform tunneling spectroscopy measurements. We use field-effect transistor configuration with four probe contacts (two tunnel and two ohmic) and bottom gates. Bandgap values extracted from tunneling measurements match the values estimated from the diameter value within the zone-folding approximation. We also observe the splitting of Van-Hove singularities of the density of states under an axial magnetic field.

Carbon nanotubes are unique flexible objects for one-dimensional electronic physics research and at the same time the promising material platform for nano-electronics and photonics. Substantial results have been achieved in applications of both individual CNTs and CNT films as the sensitive element of THz- and infrared- photodetectors[1–3] and chemical[4,5] and biosensors.[6] Observation of surface plasmons[7,8] in individual nanotubes and CNT films[9] makes them perspective for plasmonic spectrometers and interferometers.[10] Another potential application is the fully CNT-based transistor logic on microchips.[11–15]

One of the obstacles impeding integration of CNTs into commercial products is the inability to predict the electronic properties of a given CNT under specific conditions (pressure, atmosphere chemical composition, dielectric environment, etc.). In particular, it is related to a lack of systematic studies of the CNT band structure and its relation to the atomic structure of a CNT and external parameters. At the same time, there is evidence that the bandgap of a semiconducting CNT depends not only on the diameter but also on the dielectric environment and related screening of the electron–electron interactions.[16–18] The band gap of semiconductor CNTs determined from optical and tunneling experiments may differ, as it was mentioned in the beginning of the 2000s.[19,20] These differences were explained by the effects of electron–electron interactions.[16] Note that most of the experimental band structure measurement techniques are not applicable to individual nanotubes. Scanning tunneling microscopy (STM) was used for CNS spectroscopy starting from the pioneering works in 1998.[21,22] Using STM implies that the electron–electron interactions are screened by a metal substrate on which CNTs are located.

The major parameter of a semiconductor is the bandgap. Some transport experiments have indicated that the bandgap of a CNT is sensitive to the dielectric environment[18] due to electron–electron interaction screening. These correlations in CNTs remain poorly explored both experimentally and theoretically. STM does not allow for sufficient tunability of the experimental conditions (dielectric environment, etc.). Optical experiments rely on the separation of CNTs with a certain atomic structure (chirality), which is impossible in the case of few chiralities. Instead of STM, a properly fabricated tunnel

contact allows one to measure the CNT's tunneling density of states (DOS).[23] This approach was scarcely used by now. In this paper, we describe a reproducible and reliable method of tunneling contacts fabrication to a CNT. We demonstrate that such contacts may be used to probe the density of states of an individual nanotube. Our method has advantages over the so-called van-der-Waals gap tunneling spectroscopy[24] that introduces inevitable bending of the nanotubes and does not allow controlling the transparency of the tunneling barrier.

We observe the corresponding maxima of the differential conductivity and verify that they are related to the Van-Hove singularities (VHSs) of the DOS at the CNT band edges. This conclusion is based on the dependence of the device differential conductance on both the source-drain and gate voltage. We also measured the I–V curves in the magnetic field and observed the splitting of the VHS in an axial magnetic field as predicted back in 1993[25,26] and discussed in later works.[27–29] We, thus, confirm that the tunneling contact can be easily fabricated and used as an *in situ* probe of the band structure of an individual CNT. We also report on an unexpected dependence of the differential conductance of a CNT between two tunneling contacts on the source-drain and gate voltage.

We have fabricated several devices with nanotubes that have diameters about 4–6 nm. These CNTs have two to three walls, so that the Coulomb interactions are screened and the transport occurs via the outer CNT.[30] Each of our samples consists of one individual carbon nanotube with two tunnel and two ohmic contacts perpendicular to the axis of the tube [see Fig. 1(b)]. This whole structure is made in the field effect transistor configuration with *Si* p-doped back gate. The channel length between the contacts is in range of 1–2 μm depending on the device.

For the synthesis of CNTs, a home-made chemical vapor deposition (CVD) reactor was used. The synthesis method described in detail

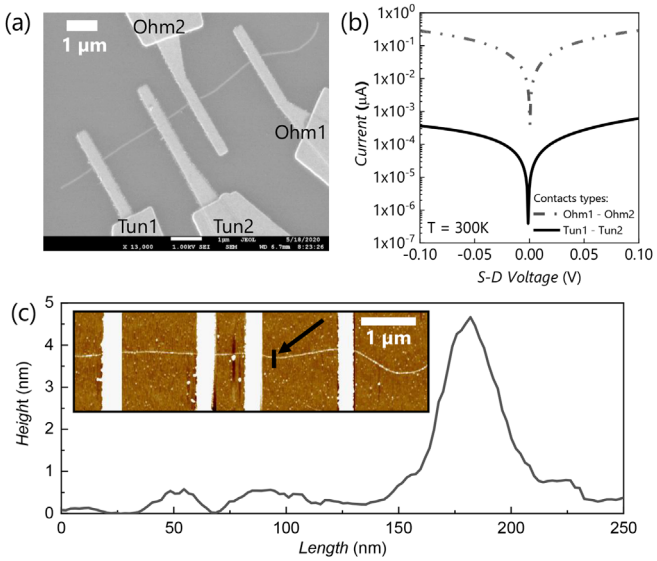

FIG. 1. Device 1. (a) SEM-picture of the device. (b) I–V curve is taken modulo measured between two pairs of contacts: Ohm1–Ohm2 and Tun1–Tun2 at room temperature by the probe station. (c) Height profile across nanotubes obtained by AFM. Inset: AFM-picture of the device. Black arrow indicates on black line along which was obtained the height profile.

in Refs. 23, 31, and 32 was shown to produce CNTs with diameter in the range from 1.5 to 5 nm on a highly doped silicon substrate with 500 nm thermal-grown SiO_2. The catalyst was a suspension in isopropyl alcohol, consisting of $Fe(NO_3)_3$: MoO_2: Al_2O_3. The synthesis process was carried out at $T = 950$ in several stages using H_2, CH_4, and Ar at atmospheric pressure. After the synthesis, the CNTs were visualized with scanning electron microscopy (SEM) to locate long straight tubes suitable for making two ohmic contacts and two tunnel contacts [Fig. 1(b)]. To make ohmic contacts, e-beam lithography and e-beam evaporation techniques were used to form 25 nm thick golden film electrodes. Importantly, at this step, no adhesion layer for gold was used. It is known that the adhesion layer is not really needed for gold sputtered onto a small area. The bigger parts sputtered afterward with an adhesion layer prevent golden contacts to CNTs from detaching. For the tunnel contact, we adopted the process for Josephson junction fabrication described in Ref. 33. Namely, a 1–2 nm thick aluminum film was e-beam evaporated through a lithographically defined mask. After deposition of aluminum, pure oxygen was injected into the chamber to acidify the film (see Ref. 23 for more details). After oxygen was evacuated from the chamber, 25 nm of gold was e-beam evaporated. It is important to note that due to a small contact area in our devices (below $10^{-2}\mu m^2$), they are not affected by the frequent problems with thin aluminum oxide films such as pinholes and inhomogeneous areas.[34] As we see from Figs. 1(b) and 5(d), a tunneling contact reduces conductance of the CNT device at room temperature about ten times. No features are observed at the IV curves obtained at room temperature due to fundamental uncertainty in energy of about 25 meV.

All electronic transport measurements were made using a commercial current preamplifier with source-drain (V_{sd}) and gate (V_g) voltages applied using a standard data acquisition system. G_{diff} was obtained by numerical differentiation of the I(V_{sd}) curves. Low temperature and high magnetic field measurements were performed using the Cryogenic CFMS-16 system. Initial characterization of our devices starts with measurement of the static conductance ($G = I/V$) for $V_{sd} = 10$ mV as a function of the gate voltage.

We selected devices, Fig. 5(c), for which this dependence is typical for semiconducting nanotubes with a bandgap of few hundred meV or larger. We next measured I–V curves at room temperature between ohmic–ohmic and tunnel–tunnel contacts. For most devices, the conductance at $V_{sd} = 50$ mV for the tunnel–tunnel pair is about two or three orders of magnitude smaller than for the ohmic–ohmic pair [see Figs. 1(b) and 5(d)]. Such a difference in the conductance indicates that the tunnel contacts work properly. To justify this conclusion, low temperature measurements were carried out.

In order to establish the relation between the differential conductance G_{diff} of our devices and the CNT density of states, we investigate the dependence of G_{diff} on both the source-drain voltage V_{sd} and the back gate voltage V_g. The data presented in Fig. 2 illustrate the results of what is close to a classical tunneling spectroscopy experiment. The section of the nanotube we probe here is connected to one ohmic and one tunneling contact. The data shown in Figs. 2(a) and 2(b) were obtained at 5 K temperature. The maxima of the differential conductance are clearly seen. Their positions are not sensitive to the gate voltage. We argue that these maxima occur when the Fermi level of the metal in the tunneling contact is aligned with the band edge in the nanotube. We note that the maxima in Figs. 2(a) and 2(b) of G_{diff} are

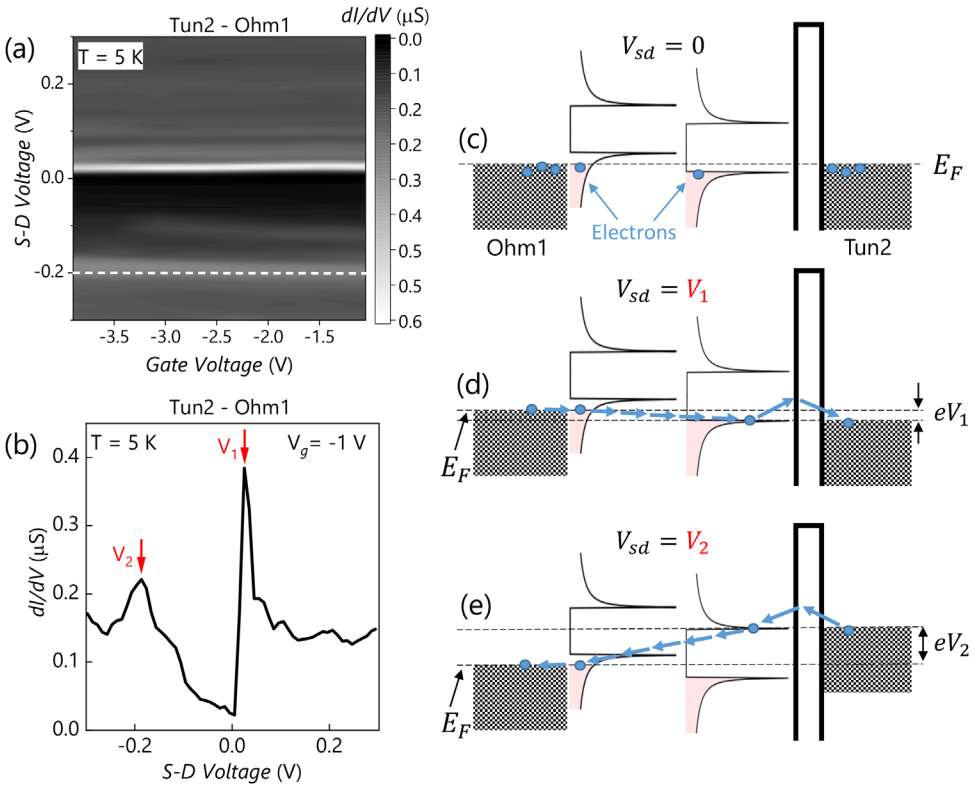

FIG. 2. Transport in device 1 between one tunneling and ohmic contacts. (a) Differential conductance as a function of the gate voltage and the source-drain voltage. (b) Differential conductance as a function of the source-drain voltage. Red arrows show maxima of G_{diff}, associated with enhanced tunneling into the CNT. (c)–(e) Energy band diagrams illustrating band alignment at zero V_{sd} (c), $V_{sd} = V_1$ (d), and $V_{sd} = V_1$ (e). Solid blue arrows illustrate tunneling, and dotted ones illustrate energy relaxation in the nanotube. The valence band of the CNT close to the ohmic contact is not filled due to contact doping.

not symmetrical about zero. This is a manifestation of the intrinsic doping of the tube.[21,22] Importantly, the tunneling conductance G_{diff} is sensitive to the doping level right in the contact area that cannot be changed via electrostatic gating. Therefore, the positions of these maxima are not sensitive to the gate voltage value. The band edges of the CNT close to the ohmic contact are shifted due to contact doping, so the carriers enter the CNT from the metal practically without any scattering. Transmission through the tunneling contact is significantly enhanced when the contact Fermi level is aligned with the conduction band edge for negative V_{sd} (V_2) and with the valence band edge for positive V_{sd} (V_1). The energy diagrams illustrating this statements are shown in Figs. 2(c)–2(e). We evaluate the bandgap of the CNT as the distance between the G_{diff} maxima ≈200 meV.

If there is no voltage drop across the ohmic contact and the CNT, the voltage drop across the tunneling contact is equal to V_{sd}. This assumption is further confirmed when the differential conductance of the CNT between two tunneling contacts is probed as a function of both gate and source-drain voltages [see the data in Figs. 3(a) and 3(b)]. In this case, we can distinctly see two G_{diff} maxima for gate voltage independent V_{sd} values as horizontal lines in Fig. 3(a) and arrows in Fig. 3(b). In the case of two tunneling contacts, the G_{diff} maxima should be observed when the Fermi level of the contact metal matches the CNT band edge on both sides [see the diagram (d) and (e) in Fig. 3] of the device. In this case, the maxima should be observed at $V_{sd} = \pm E_g/e$, where e is the elementary charge. This turns out to be the case in our experiments as seen from the plot in Figs. 3(a) and 3(b).

As seen from the 2D plot in Fig. 3(a), there some maxima of G_{diff} depend on the applied gate voltage. They cannot be related to the density of states in the contact area of the nanotube. Interestingly, they form a pattern characteristic for a Coulomb blockade (CB). The size of the "diamonds" would be the same in the case of CB in a CNT with a length of about 100 nm or less, while we deal with a ∼2 μm long section of a CNT. At this point, we have no explanation to the origin of the observed pattern.

The value of the bandgap extracted from the G_{diff} vs V_{sd} curves ($E_g \approx 200$ meV) is consistent with the diameter of the nanotube that was measured with atomic force microscopy (AFM). The diameter d of the CNT discussed to date is found to be 4.5 ± 0.5 nm. According to the zone-folding approximation, the bandgap of a single carbon nanotube should follow the relation:[22]

$$E_g = \frac{2\gamma_0 a_{c-c}}{d}, \tag{1}$$

where γ_0 is the nearest-neighbor energy overlap integral[35] and $a_{cc} = 0,142$ nm is the distance between the neighboring carbon atoms. The value of γ_0 is known to be between 2.5 and 3 eV.[21,36] We assume it to be about 2.8 eV based on the commonly excepted value of the Fermi velocity in graphene $v_f = 3/2\gamma_0|a| = 10^6$ m/s.

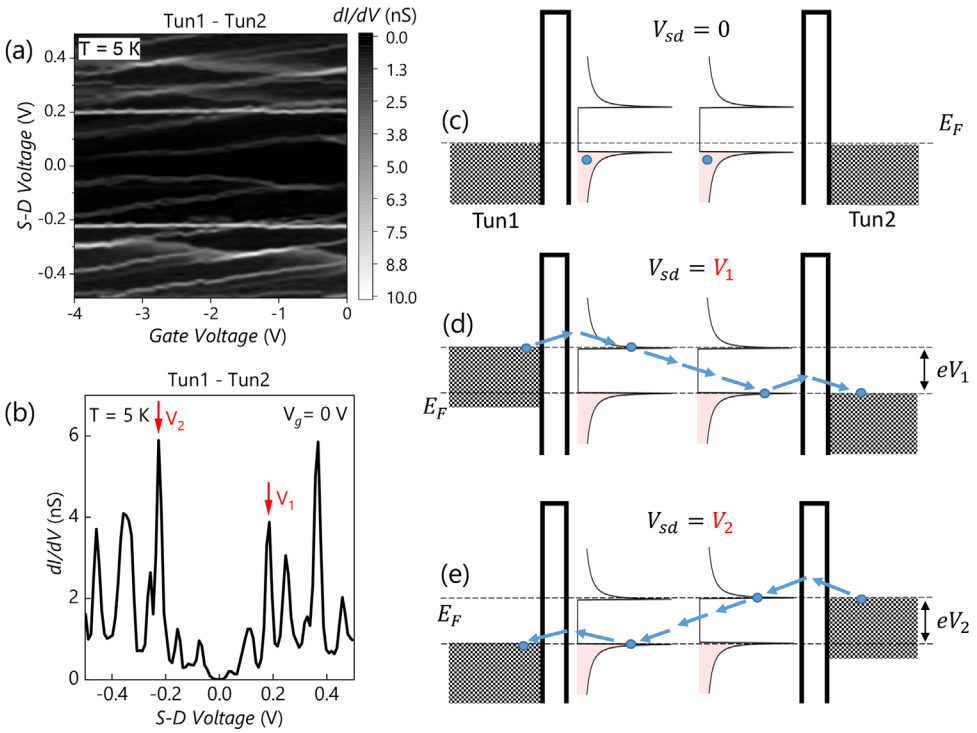

FIG. 3. Transport in device 1 between two tunneling contacts. (a) Differential conductance as a function of the gate voltage and the source-drain voltage. (b) Differential conductance as a function of the source-drain voltage. Red arrows show the maxima of G_{diff} associated with enhanced tunneling into the CNT. (c)–(e) Energy band diagrams illustrating the band alignment at $V_{sd} = 0$ (c), $V_{sd} = V_1$ (d), and $V_{sd} = V_1$ (e). Solid blue arrows illustrate tunneling events, and dotted ones show energy relaxation in the nanotube.

In this case, we estimate the bandgap of a semiconducting CNT to be equal to 0.18 eV, close enough to the value obtained from the dV/dI vs V_{sd} curves. Importantly, Eq. (1) can be used only as rough estimate of a MWNT bandgap. Due to intershell coupling, the bandgap of MWNTs with the same diameter may be different (see Refs. 41–43 for some of the theoretical results on the matter). Accuracy of our current setup does not allow for getting information on the inner structure of the studied MWNT based on the obtained bandgap value.

The relation between the differential conductance G_{diff} of our devices and the CNT density of states motivates us to perform tunneling DOS measurements under the axial magnetic field. It is well established theoretically that the axial magnetic field lifts the degeneracy between the K and K′ bands of the CNT band structure. This results in splitting of the VHS of the DOS of a CNT. Figure 4 illustrates this effect within the zone folding approximation.

Under zero magnetic field allowed values of the wave-vector component $k_\perp$ perpendicular to the CNT axis are defined by the condition

$$k_\perp L = 2\pi n, \tag{2}$$

with n being an integer and $L = \pi d$ being the CNT circumference. In magnetic field B parallel to the CNT axis, this condition is replaced with

$$k_\perp L + B\pi d^2/4\phi_0 = 2\pi n, \tag{3}$$

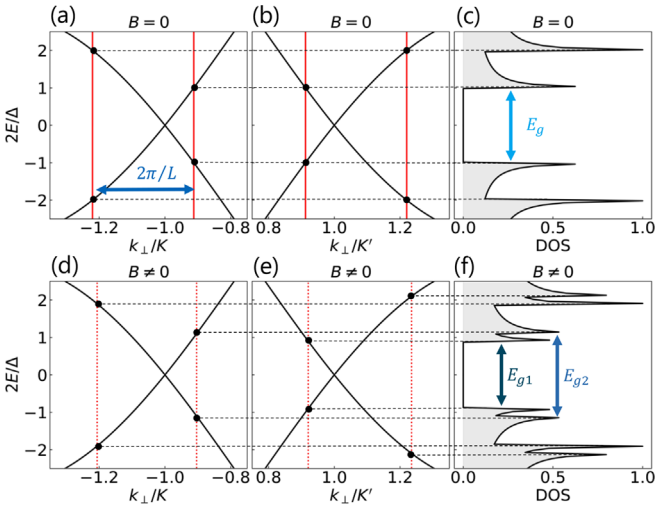

FIG. 4. Theoretical explanation of the CNT DOS splitting in the axial magnetic field. The upper row shows the dispersion law near K and K' points (a) and (b), and density of states (c) for a single semiconducting CNT when the magnetic flux along the tube axis is zero. Bottom row shows dispersion law near K and K' points (d) and (e), and density of states (f) when a magnetic field is applied along the tube axis. Red lines are zone folding crossing lines. When the magnetic field is applied along the tube axis, zone folding crossing lines are shifted in different directions (d) and (e); thus, the valley degeneracy is lifted and the peaks of the density of states split (f).

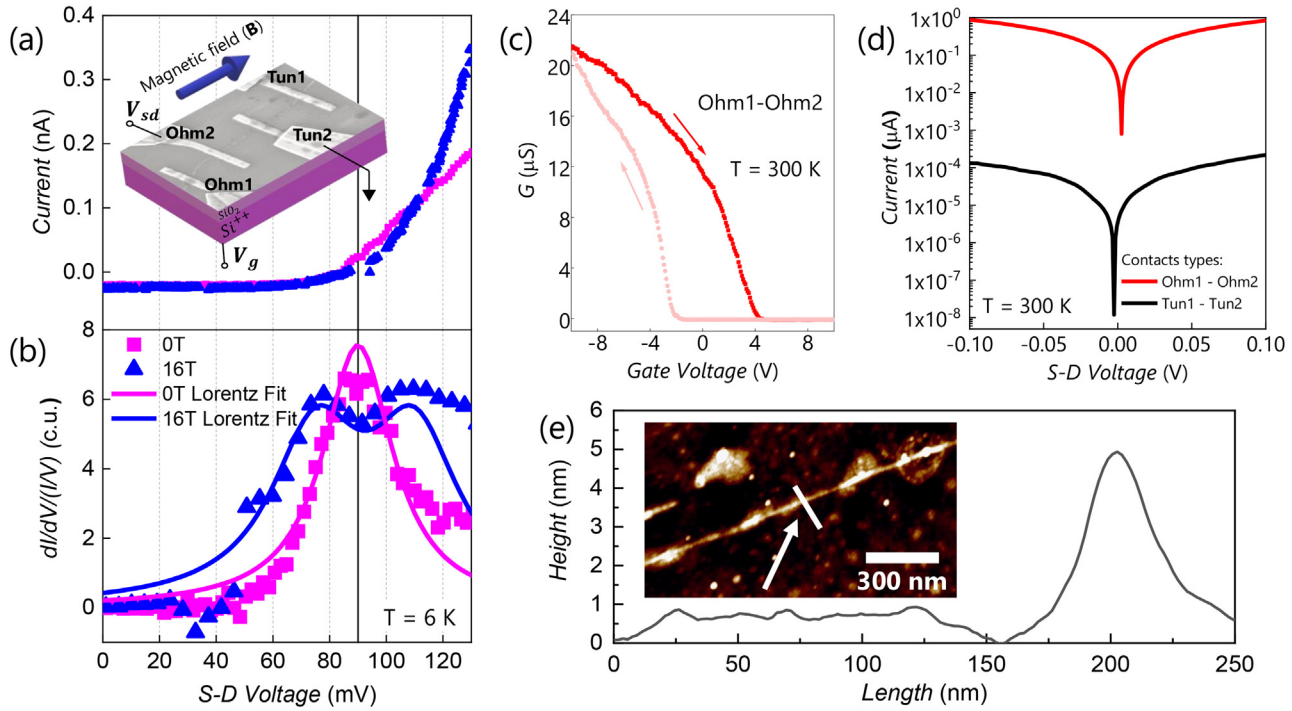

FIG. 5. Device 2. (a) I–V curves measured between Ohm2 and Tun2 with and without magnetic fields directed along the axis of the tube: red curve ($B = 16$T) and black curve ($B = 0$T). Inset: SEM-picture of the device with simple experiment scheme. (b) Black and red points shows *I–V* curves from Fig. 5(a) numerically differentiated and multiplied and by *V/I*. Black and red lines are the Lorenz-fits. In magnetic field $B = 16$T, the DOS peak splits into two peaks. Difference of V_{sd} between these peaks is ∼40 mV. (c) Transistor characteristics of the device: conductance (G) depending on the gate voltage shows us that the tube in device 2 is semiconducting (after $Vg > 4V$ conductance is equal to zero). Different shades of red and arrows show the gate voltage changing direction. The observed hysteresis is a common phenomenon in such transistor structures based on CNTs[37,38] and graphene.[39,40] It is associated with the recharge of traps in the near-surface layer of silicon oxide and the recharge of contaminations and water molecules on the CNT surface. (d) I–V curve is taken modulo measured between two pairs of contacts: Ohm1–Ohm2 and Tun1–Tun2 at room temperature by the probe station. (e) Height profile across the nanotube obtained by AFM. Inset: AFM-picture of the device central part between Tun2 and Ohm2 contacts. White arrow indicates on white line along which was obtained the height profile.

with $\phi_0 = h/e$ being the magnetic flux quantum. As shown in Fig. 4, band edges shift up for one of the K, K' bands and down for the one. While the CNT bandgap change under the axial magnetic field has been reported in several works,[27,28,44,45] the VHS splitting was only observed by optical methods using a large number of CNTs in suspension.[46] Here, we observe this effect simply by measuring the differential conductance of a tunnel contact as a function of the source-drain voltage. Figure 5(b) compares G_{diff} (V_{sd}) curves of another CNT based device measured at 6 K under magnetic fields of 0 and 16 T. Note that the maximum of G_{diff} obtained at zero magnetic field is split into two so that one is shifted to lower V_{sd}, while the other one is shifted to higher one. One can extract the nanotube diameter from the magnitude of spitting using the relation

$$\Delta V_{sd} = \Delta E/e = Bdv_F/2. \quad (4)$$

Based on the data shown in Fig. 5(b), we estimate the diameter value to be 5 ± 0.5 nm, which is close to the value obtained using AFM. Importantly, the VHS splitting under axial magnetic fields has never been demonstrated in an individual CNT so far.

To summarize, we have implemented tunneling contacts into several devices based on individual CNTs. Our results prove that a tunneling contact can be used as a tool for *in situ* measurements of a CNT bandgap. The approach described here is expected to give new results in the case of the so-called quasi-metallic CNTs that have a curvature-induced bandgap of the order of 10 meV. It can be further used for quantitative analysis of the electron–electron interactions on the CNT band structure. We also demonstrate VHS splitting resulting from the magnetic field-driven lifting of valley degeneracy in an individual CNT.

The work of Y.M. (sample design and fabrication) was funded by RFBR, Project No. 20-32-90224. The transport measurements under magnetic fields were conducted at the Shared Facility Centre of the P.N. Lebedev Physical Institute and supported by the Russian Science Foundation via Grant No. 21-72-20050. G.F. acknowledges support of the RSF under Project No. 21-79-20225 (data analysis and interpretation).

AUTHOR DECLARATIONS

Conflict of Interest

The authors have no conflicts to disclose.

DATA AVAILABILITY

The data that support the findings of this study are available from the corresponding author upon reasonable request.

REFERENCES

[1]M. Freitag, Y. Martin, J. A. Misewich, R. Martel, and P. Avouris, Nano Lett. **3**, 1067 (2003).
[2]H. Chen, N. Xi, K. W. C. Lai, C. K. M. Fung, and R. Yang, IEEE Trans. Nanotechnol. **9**, 582 (2010).
[3]G. Fedorov, I. Gayduchenko, N. Titova, A. Gazaliev, M. Moskotin, N. Kaurova, B. Voronov, and G. Goltsman, Phys. Status Solidi B **255**, 1700227 (2018).
[4]T. Zhang, M. Nix, B.-Y. Yoo, M. Deshusses, and N. Myung, Electroanalysis **18**, 1153 (2006).
[5]T. Zhang, S. Mubeen, N. V. Myung, and M. A. Deshusses, Nanotechnology **19**, 332001 (2008).
[6]K. Balasubramanian and M. Burghard, Anal. Bioanal. Chem. **385**, 452 (2006).
[7]Z. Shi, X. Hong, H. A. Bechtel, B. Zeng, M. C. Martin, K. Watanabe, T. Taniguchi, Y.-R. Shen, and F. Wang, Nat. Photonics **9**, 515 (2015).
[8]Q. Zhang, E. H. Hároz, Z. Jin, L. Ren, X. Wang, R. S. Arvidson, A. Lüttge, and J. Kono, Nano Lett. **13**, 5991 (2013).
[9]V. Ryzhii, T. Otsuji, M. Ryzhii, V. G. Leiman, G. Fedorov, G. N. Goltzman, I. A. Gayduchenko, N. Titova, D. Coquillat, D. But, W. Knap, V. Mitin, and M. S. Shur, J. Appl. Phys. **120**, 044501 (2016).
[10]Y. Matyushkin, S. Danilov, M. Moskotin, G. Fedorov, A. Bochin, I. Gorbenko, V. Kachorovskii, and S. Ganichev, Opt. Express **29**, 37189 (2021).
[11]S. J. Tans, A. R. M. Verschueren, and C. Dekker, Nature **393**, 49 (1998).
[12]R. Martel, T. Schmidt, H. R. Shea, T. Hertel, and P. Avouris, Appl. Phys. Lett. **73**, 2447 (1998).
[13]A. Bachtold, Science **294**, 1317 (2001).
[14]Z. Chen, Science **311**, 1735 (2006).
[15]G. Hills, C. Lau, A. Wright, S. Fuller, M. D. Bishop, T. Srimani, P. Kanhaiya, R. Ho, A. Amer, Y. Stein, D. Murphy, Arvind, A. Chandrakasan, and M. M. Shulaker, Nature **572**, 595 (2019).
[16]C. Zhu, Y. Liu, J. Xu, Z. Nie, Y. Li, Y. Xu, R. Zhang, and F. Wang, Sci. Rep. **7**, 11221 (2017).
[17]F. Shao, F. X. Zha, C. B. Pan, J. Shao, X. L. Zhao, and X. C. Shen, Phys. Rev. B **89**, 085423 (2014).
[18]L. Aspitarte, D. R. McCulley, A. Bertoni, J. O. Island, M. Ostermann, M. Rontani, G. A. Steele, and E. D. Minot, Sci. Rep. **7**, 8828 (2017).
[19]S. M. Bachilo, Science **298**, 2361 (2002).
[20]T. W. Odom, J.-L. Huang, P. Kim, and C. M. Lieber, J. Phys. Chem. B **104**, 2794 (2000).
[21]J. W. G. Wilder, L. C. Venema, A. G. Rinzler, R. E. Smalley, and C. Dekker, Nature **391**, 59 (1998).
[22]T. W. Odom, J.-L. Huang, P. Kim, and C. M. Lieber, Nature **391**, 62 (1998).
[23]Y. Matyushkin, N. Kaurova, B. Voronov, G. Goltsman, and G. Fedorov, Fullerenes, Nanotubes Carbon Nanostruct. **28**, 50 (2020).
[24]D.-H. Choi, S. M. Lee, D.-W. Jeong, J.-O. Lee, D. H. Ha, M.-H. Bae, and J.-J. Kim, Molecules **26**, 2128 (2021).
[25]H. Ajiki and T. Ando, J. Phys. Soc. Jpn. **62**, 1255 (1993).
[26]H. Ajiki and T. Ando, Physica B **201**, 349 (1994).
[27]E. D. Minot, Y. Yaish, V. Sazonova, and P. L. McEuen, Nature **428**, 536 (2004).
[28]U. Coskun, T.-C. Wei, S. Vishveshwara, P. Goldbart, and A. Bezryadin, Science **304**, 1132 (2004).
[29]C. Strunk, B. Stojetz, and S. Roche, Semicond. Sci. Technol. **21**, S38 (2006).
[30]M. R. Buitelaar, A. Bachtold, T. Nussbaumer, M. Iqbal, and C. Schönenberger, Phys. Rev. Lett. **88**, 156801 (2002).
[31]J. Kong, H. T. Soh, A. M. Cassell, C. F. Quate, and H. Dai, Nature **395**, 878 (1998).
[32]N. R. Franklin, Y. Li, R. J. Chen, A. Javey, and H. Dai, Appl. Phys. Lett. **79**, 4571 (2001).
[33]L. J. Zeng, T. Greibe, S. Nik, C. M. Wilson, P. Delsing, and E. Olsson, J. Appl. Phys. **113**, 143905 (2013).
[34]B. Dlubak, M.-B. Martin, C. Deranlot, K. Bouzehouane, S. Fusil, R. Mattana, F. Petroff, A. Anane, P. Seneor, and A. Fert, Appl. Phys. Lett. **101**, 203104 (2012).
[35]P. R. Wallace, Phys. Rev. **71**, 622 (1947).
[36]R. B. Weisman and S. M. Bachilo, Nano Lett. **3**, 1235 (2003).
[37]R. S. Park, M. M. Shulaker, G. Hills, L. S. Liyanage, S. Lee, A. Tang, S. Mitra, and H.-S. P. Wong, ACS Nano **10**, 4599 (2016).
[38]S. Kar, A. Vijayaraghavan, C. Soldano, S. Talapatra, R. Vajtai, O. Nalamasu, and P. M. Ajayan, Appl. Phys. Lett. **89**, 132118 (2006).
[39]H. Wang, Y. Wu, C. Cong, J. Shang, and T. Yu, ACS Nano **4**, 7221 (2010).
[40]Y. G. Lee, C. G. Kang, U. J. Jung, J. J. Kim, H. J. Hwang, H.-J. Chung, S. Seo, R. Choi, and B. H. Lee, Appl. Phys. Lett. **98**, 183508 (2011).
[41]T. Ando, J. Phys. Soc. Jpn. **74**, 777 (2005).
[42]J.-C. Charlier, X. Blase, and S. Roche, Rev. Mod. Phys. **79**, 677 (2007).
[43]D. Mtsuko, A. Koshio, M. Yudasaka, S. Iijima, and M. Ahlskog, Phys. Rev. B **91**, 195426 (2015).
[44]G. Fedorov, A. Tselev, D. Jiménez, S. Latil, N. G. Kalugin, P. Barbara, D. Smirnov, and S. Roche, Nano Lett. **7**, 960 (2007).
[45]G. Fedorov, P. Barbara, D. Smirnov, D. Jiménez, and S. Roche, Appl. Phys. Lett. **96**, 132101 (2010).
[46]S. Zaric, Science **304**, 1129 (2004).